Materials Transactions, Vol. 48, No. 7 (2007) pp. 1759 to 1764
Special Issue on Bulk Metallic Glasses —Selected Papers from the Fifth International Conference on Bulk Metallic Glasses (BMGV)

Characterization of Shear Banding in La-Based Bulk Metallic Glasses through Indentation

Wei Peng[1], Bingchen Wei[1,*], Taihua Zhang[2], Yuan Liu[1] and Lei Li[1]

[1]*National Microgravity Laboratory, Institute of Mechanics, Chinese Academy of Sciences, Beijing 100080, P. R. China*
[2]*State Key Laboratory of Nonlinear Mechanics (LNM), Institute of Mechanics, Chinese Academy of Sciences, Beijing 100080, P. R. China*

$La_{64}Al_{14}(Cu,Ni)_{22}$, $La_{63.1}Al1_{5.2}(Cu,Ni)_{21.7}$, $La_{57.6}Al_{17.5}(Cu,Ni)_{24.9}$, and $La_{55}Al_{25}Cu_{10}Ni_5Co_5$ bulk metallic glasses (BMGs) with low glass transition temperature (T_g) were prepared by copper-mould casting method. The homologous temperature (the ratio of room temperature to T_g) of the four BMGs ranges from 0.64 to 0.73. Plastic deformation behavior of the BMGs at various loading rates was studied by nanoindentation. The results showed that the loading rate dependency of serrated flow, which is related to the nucleation and propagation of shear bands, depends strongly on the homologous temperature. The alloys with relatively high homologous temperature exhibit an increase in flow serration with increasing loading rate, whereas, the alloys with low homologous temperature exhibit prominent serrations at low rates. No distinct shear band is observed around the indents for all alloys after nanoindentation at all the studied loading rates. Alternately, shear band pattern are characterized through macro-indentation, which shows that shear band spacing decreases with the increase of the homologous temperature.
[doi:10.2320/matertrans.MJ200761]

(Received December 1, 2006; Accepted January 9, 2007; Published June 25, 2007)

Keywords: *Bulk metallic glass, plastic deformation, shear band, nanoindentation*

1. Introduction

The plastic deformation of bulk metallic glasses (BMGs) can be classified by either inhomogeneous or homogeneous deformation.[1,2] Homogeneous deformation in metallic glasses usually takes place at high temperatures. The deformation behavior of BMGs near glass transition temperature (T_g) can be Newtonian or non-Newtonian, depending on temperature and imposed strain rate.[3–7] Inhomogeneous deformation usually occurs at low temperatures (*e.g.* room temperature) or at a larger strain rates, and is characterized by the formation of localized shear bands, followed by their rapid propagation, and catastrophic fracture. In constrained modes of loading (*e.g.*, compression, bending or indentation), global plastic deformation at room temperature is possible, where flow is typically found to be serrated.[8–11] It is originally assumed that the change-over of the type of flow is controlled by the homologous temperature (T_h: the ratio of testing temperature to T_g): for $T_h \leq 0.65 \sim 0.70$ the flow is localized whereas at higher temperatures homogeneous flow arises.[1,2] This point of view has gained wide acceptance despite the direct experimental evidence on shear banding feature around the change-over regime is still quite limited.

Recently, nanoindentation experiments have increasingly being used to evaluate the mechanical response of metallic glasses. It is found that the serrated flow during nanoindentation at room temperature strongly depends on the indentation strain rate, with lower rates promoting more prominent serrations in Pd-, Zr-, La-, Nd-, Mg- and Cu-based BMGs.[10–16] The T_h value for these BMGs at room temperature ranges from 0.41 to 0.72. On the other hand, it is also reported that higher loading rate promotes more prominent serration in a Ce-based BMG with $T_h = 0.73$, while no serration appear in the alloys with $T_h > 0.8$.[17] The serrated flow during the plastic deformation in metallic glasses is related to the nucleation and propagation of shear bands. For gaining a further insight on the microscopic mechanism of the transition of the flow type in BMGs, we focus on the shear banding feature of BMGs around the change-over temperature in one alloy system. For this aim, the serrated flow during nanoindentation at various loading rates in four La-based BMGs with the T_h value from 0.64 to 0.73 was studied.

2. Experimental Procedures

Ingots of $La_{64}Al_{14}(Cu,Ni)_{22}$, $La_{63.1}Al1_{5.2}(Cu,Ni)_{21.7}$, $La_{57.6}Al_{17.5}(Cu,Ni)_{24.9}$, and $La_{55}Al_{25}Cu_{10}Ni_5Co_5$ (at%) alloys were prepared by arc-melting the pure elements with purities ranging from 99.5% to 99.99% together under a purified argon atmosphere. Cylindrical rods with 3 mm diameter were produced by chill-casting into a copper mold. The structure of the samples was characterized by X-ray diffraction (XRD) using Cu $K\alpha$ radiation. Thermal analysis was performed with a Perkin-Elmer DSC 7 differential scanning calorimeter at a heating rate of 20 K/min under argon atmospheres. Nanoindentation tests were conducted using an MTS Nano Indenter XP™ with a Berkovich diamond tip under a load control mode. The specimens were polished to mirror finish before measurements. The loading procedure consisted of five subsequent steps: (1) loading to a peak depth at a selected loading rate; (2) holding the load for 10 s at the peak depth; (3) unloading to 90% of the peak load at the rate same to the loading one; (4) holding load for 10 s for thermal drift calibration; (5) unloading completely. Four loading rates were used in the experiments (0.075 mN/s, 0.2 mN/s, 0.5 mN/s and 1 mN/s). The thermal drift of the instrument was below 0.05 nm/s. At least six indentations were made for each test. All the tests were carried out at room temperature (293 K). Indentation tests were also done using conical diamond tip ($\theta = 60^\circ$) under standard Rockwell hardness measurement procedures (600 N load).

*Corresponding author, E-mail: weibc@imech.ac.cn

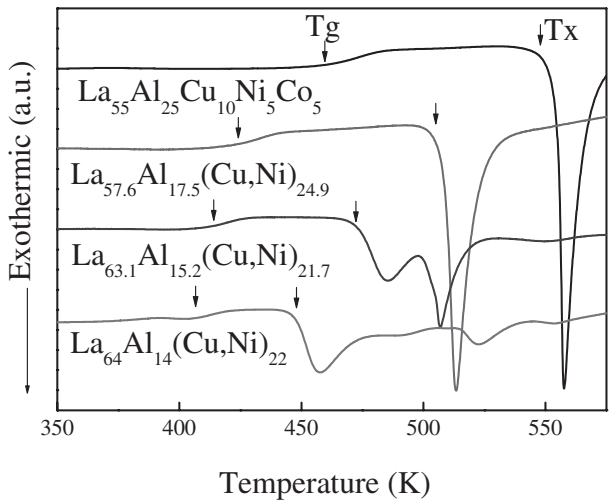

Fig. 1 DSC curves for the four BMGs at the heating rate of 20 K/min.

3. Results and Discussion

XRD patterns of the as-cast $La_{64}Al_{14}(Cu,Ni)_{22}$, $La_{63.1}Al1_{5.2}(Cu,Ni)_{21.7}$, $La_{57.6}Al_{17.5}(Cu,Ni)_{24.9}$, and $La_{55}Al_{25}Cu_{10}Ni_5Co_5$ alloys with 3 mm diameter exhibit typical amorphous structure under the detection limit of XRD (not shown here). The DSC results obtained at a heating rate of 20 K/min for the as-cast four BMGs are shown in Fig. 1. All BMGs show an endothermic reaction caused by glass transition, followed by an exothermic reaction caused by crystallization. The onset temperature of glass transition (T_g), the crystallization temperature (T_x), the width of supercooled liquid region ($\Delta T = T_x - T_g$) and homologous temperature ($T_h = RT/T_g$; RT is room temperature of 293 K) of the four BMGs are listed in Table 1. It can be seen that T_h is 0.73, 0.71, 0.69 and 0.64 for $La_{64}Al_{14}(Cu,Ni)_{22}$, $La_{63.1}Al1_{5.2}(Cu,Ni)_{21.7}$, $La_{57.6}Al_{17.5}(Cu,Ni)_{24.9}$, and $La_{55}Al_{25}Cu_{10}Ni_5Co_5$ alloy, respectively. The T_g, T_x and ΔT values of the four BMGs agree well with the reported results.[18)]

Mechanical properties and plastic deformation behaviors of the four BMGs are investigated through nanoindentation. The measured hardness and elastic modulus of each alloy are also listed in Table 1. Typical load-displacement (*P-h*) curves during nanoindentation at various loading rates for the four BMGs are presented in Fig. 2. The origin of each curve is displaced for clearer observation. It can be seen that the hardness of the four La-based BMGs all depends on the loading rate, and increases gradually from 3.12 GPa at 0.075 mN/s to 3.22 GPa at 1.0 mN/s for $La_{55}Al_{25}Cu_{10}Ni_5Co_5$ alloy, while 1.99 GPa at 0.075 mN/s to 2.27 GPa at 1.0 mN/s for $La_{64}Al_{14}(Cu,Ni)_{22}$ alloy, respectively. Hardness is relatively insensitive to the loading rate for the alloy with higher T_h. It can also be observed in Fig. 2 that, during the hold segment for 10 s at the maximum load, a creep deformation occurs for the four BMGs, which is more prominent at higher loading rates and for the alloy with high T_h. The creep displacement is about 20 nm at 1.0 mN/s for $La_{64}Al_{14}(Cu,Ni)_{22}$ alloy with the highest T_h.

It should be noted that the deformation behavior of the four BMGs strongly depends on the indentation loading rate, as shown in the loading parts of the *P-h* curves in Fig. 2. The $La_{55}Al_{25}Cu_{10}Ni_5Co_5$ BMG ($T_h = 0.64$, Fig. 2(a)) exhibits serrated *P-h* curves with many distinct displacement bursts at low loading rates, while less pronounced serrations at high loading rates. The trend of rate dependency of serration is consistent with the previous results on the same alloy.[16)] For the $La_{57.6}Al_{17.5}(Cu,Ni)_{24.9}$ BMG ($T_h = 0.69$, Fig. 2(b)), serrations are insensitive to the loading rate, and a less pronounced serrated flow is observed for all the studied loading rates. For the alloy with much lower T_g, the $La_{63.1}Al1_{5.2}(Cu,Ni)_{21.7}$ BMG ($T_h = 0.71$, Fig. 2(c)) exhibits a few displacement bursts at the lowest loading rate of 0.075 mN/s, while shows strong serrations at high rates. For the $La_{64}Al_{14}(Cu,Ni)_{22}$ BMG with the highest T_h value of 0.73 (Fig. 2(d)), the *P-h* curve at 0.075 mN/s is nearly smooth, and serrations increase with the increase of loading rate.

To further characterize the serrated flow in the load-

Table 1 T_g, T_x, ΔT, T_h, hardness and elastic modulus of the four BMGs though DSC and nanoindentation measurements.

Alloys	T_g (K)	T_x (K)	T_h	Loading Rate(mN/s)	Modulus (GPa)	Hardness (GPa)
$La_{55}Al_{25}Cu_{10}Ni_5Co_5$	461	543	0.64	0.075	55.3	3.12
				0.2	54.5	3.14
				0.5	53.1	3.21
				1	52.8	3.22
$La_{57.6}Al_{17.5}(Cu,Ni)_{24.9}$	423	500	0.69	0.075	54.0	2.64
				0.2	50.6	2.76
				0.5	50.0	2.80
				1	49.2	2.89
$La_{63.1}Al_{15.2}(Cu,Ni)_{21.7}$	411	468	0.71	0.075	50.8	1.95
				0.2	46.2	2.17
				0.5	43.3	2.25
				1	41.8	2.29
$La_{64}Al_{14}(Cu,Ni)_{22}$	401	449	0.73	0.075	49.2	1.99
				0.2	47.2	2.08
				0.5	45.5	2.24
				1	43.8	2.27

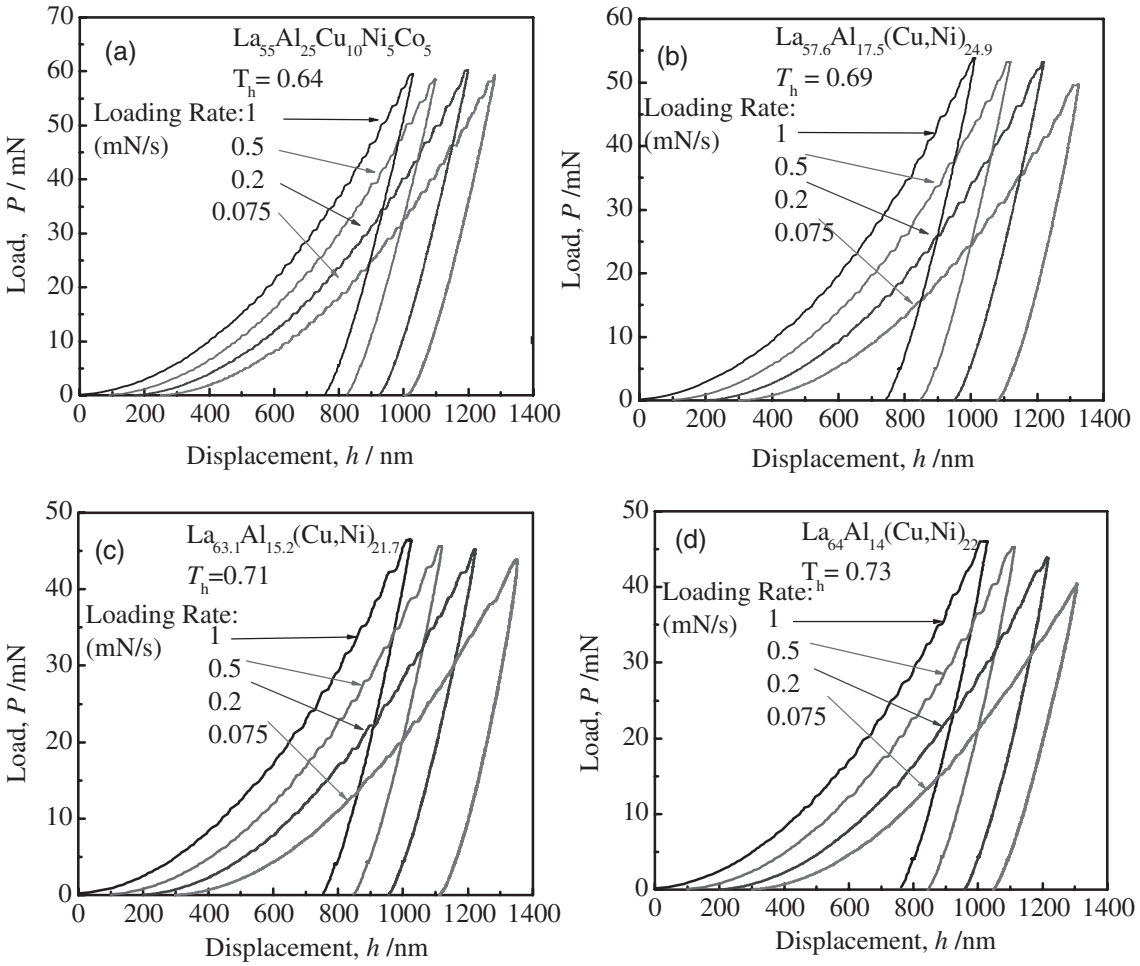

Fig. 2 Typical load-displacement (*P-h*) curves during nanoindention at various loading rates for the four BMGs: $La_{55}Al_{25}Cu_{10}Ni_5Co_5$ (a), $La_{57.6}Al_{17.5}(Cu,Ni)_{24.9}$ (b), $La_{63.1}Al1_{5.2}(Cu,Ni)_{21.7}$ (c), $La_{64}Al_{14}(Cu,Ni)_{22}$ (d).

displacement curves of the four BMGs during nanoindentation at various loading rates, the range of serrations is used to express the features of the serrations. The displacement plotted as a function of the load at various the loading rates was simulated as exponential function:

$$h_{fit} = CP^m \tag{1}$$

where, C and m are constant. The function

$$\Delta h = h_{exp} - h_{fit} \tag{2}$$

describes the range of serrations, where h_{exp} is the experimental value. Figure 3 shows Δh-h curves for the four BMGs during nannoindentation at various loading rates. It can be seen that rapid indentation leads to an increase in displacement burst number and a decrease in burst scale in the $La_{55}Al_{25}Cu_{10}Ni_5Co_5$ BMG with the lowest T_h. In contrast, in the alloys with high T_h ($La_{63.1}Al1_{5.2}(Cu,Ni)_{21.7}$ and $La_{57.6}Al_{17.5}(Cu,Ni)_{24.9}$) high loading rates promote an increase both in number and scale of the displacement bursts. These results (Fig. 2 and Fig. 3) indicate that the loading rate dependency of serration change from one trend to an opposite one in the same alloy system with various T_h values, that is, flow serration decreases with increasing loading rate for the alloy with low T_h, and increases with increasing loading rate for the high T_h alloys. The change-over T_h value is about 0.69, wherein the flow serration is relatively insensitive to the loading rate.

The flow serration during nanoindentation in BMGs is related to the nucleation and propagation of shear bands. For further understanding the deformation behavior of the La-based BMGs with various T_h values, the plastic deformation region around the indents after indentation at different loading rates was studied. Typical surface morphologies of indents for the $La_{63.1}Al1_{5.2}(Cu,Ni)_{21.7}$ BMG after indentation at 0.075 and 1.0 mN/s are shown in Fig. 4. No shear band can be seen in the alloy after nanoindentation at all the studied loading rates. The other three BMGs also exhibit the same result (not shown here) that no shear band can be seen around the indents after nanoindentation at all loading rates, irrespective of there is or not serrated flow in the *P-h* curves.

To clarify the shear band features in the La-based BMGs during indentation, macroindention tests were conducted using conical indenter at the load of 600 N. The surface morphologies of indents after macroindentation for the four BMGs are shown in Fig. 5. Distinct shear band pattern can be observed for the four BMGs around the indents. Two sets of shear planes (nearly mutually orthogonal) originate at the edge of the indent are seen in all BMGs, which follow an

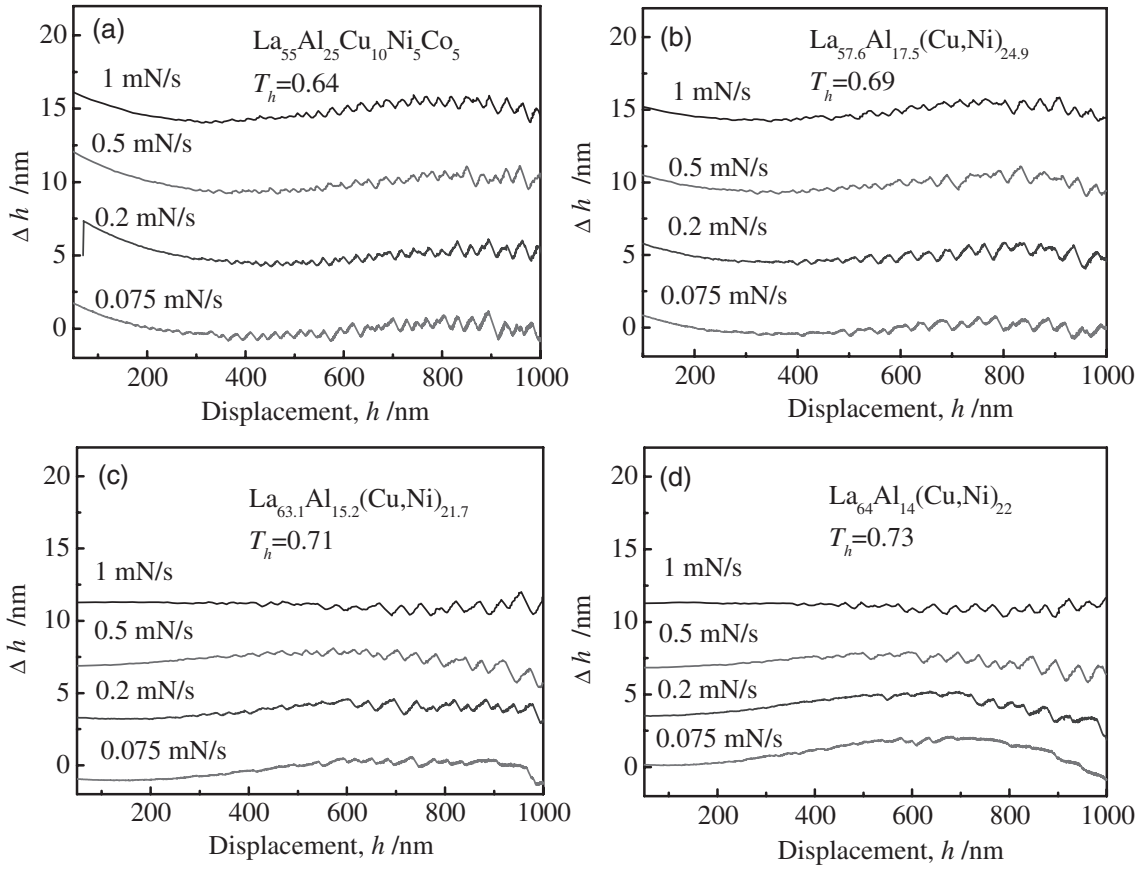

Fig. 3 Δh-h curves for the four BMGs during nannoindentation at various loading rates: $La_{55}Al_{25}Cu_{10}Ni_5Co_5$ (a), $La_{57.6}Al_{17.5}(Cu,Ni)_{24.9}$ (b), $La_{63.1}Al1_{5.2}(Cu,Ni)_{21.7}$ (c), $La_{64}Al_{14}(Cu,Ni)_{22}$ (d).

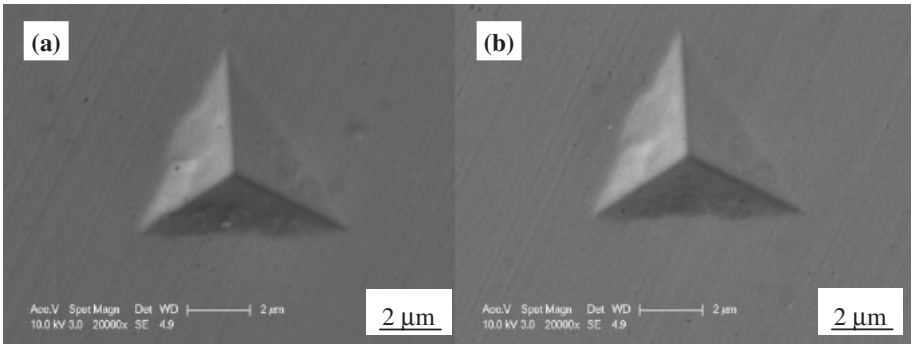

Fig. 4 Typical morphologies around the indents after nanoindentation measurements at various loading rates: 0.075 mN/s (a), 1.0 mN/s (b).

outward logarithmic spiral pattern. Though the actual applied loading rate during macroindentation is much higher than that during nanoindentation, the shear band pattern still can provide valuable information on the shear banding features of different alloys. It can be seen in Fig. 5 that the shear band number in the alloys with low T_h values is much higher than that in the high T_h alloys, whereas the shear band upsets decrease with the increase of T_h value.

The loading rate dependency of the serrated flow during nanoindentation in the present $La_{55}Al_{25}Cu_{10}Ni_5Co_5$ BMG ($T_h = 0.64$) is consistent with that of other BMG systems, *e.g.* Zr-, Pd-, Cu-, La-, and Mg-based BMGs, for which a low indentation rate promotes more pronounced serrations, and rapid indentation suppresses serrated flow.[10–16] The disappearance of prominent serrated flow at high rates was supposed to be the simultaneous operation of multiple shear bands to accommodate to rapid plastic deformation, though the increase of the number of serrations at high loading rates is not found in the *P-h* curves. However, the *P-h* curves of the four La-based BMGs in this study clearly show that the number of serrations increase significantly with the loading rate (Fig. 2 and Fig. 3). This gives a direct proof for the operation of multiple shear bands at high rates, and also accounts for the less pronounced serrations at high loading rates for the $La_{55}Al_{25}Cu_{10}Ni_5Co_5$ BMG with the lowest T_h in this work.

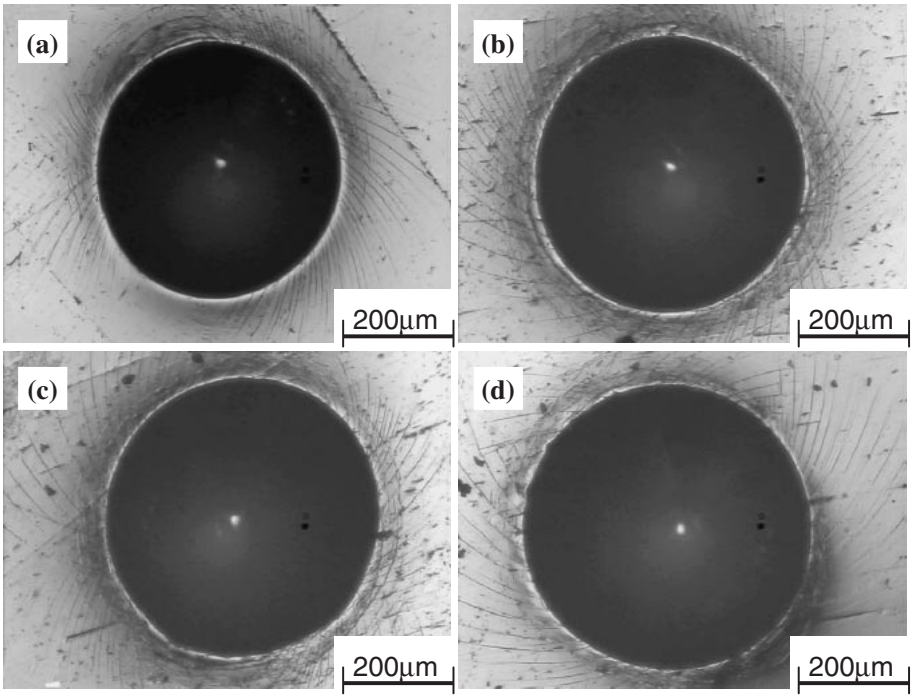

Fig. 5 Typical morphologies around the indents after macroindentation using conical indenter for the four BMGs: $La_{55}Al_{25}Cu_{10}Ni_5Co_5$ (a), $La_{57.6}Al_{17.5}(Cu,Ni)_{24.9}$ (b), $La_{63.1}Al1_{5.2}(Cu,Ni)_{21.7}$ (c), $La_{64}Al_{14}(Cu,Ni)_{22}$ (d).

It should be pointed out that the $La_{63.1}Al1_{5.2}(Cu,Ni)_{21.7}$ and $La_{64}Al_{14}(Cu,Ni)_{22}$ BMGs with high T_h values exhibit an opposite rate dependency of serrated flow during nanoindentation, wherein a smooth deformation occurs at low loading rates and prominent serrated flow appears at high rates (Fig. 2 and Fig. 3). The four La-based BMGs studied here are similar in chemical composition. The different deformation behavior during nanoindentation may be related to the difference in T_h value of the two alloys. It is generally accepted that the deformation mechanism of metallic glasses depends both on the testing temperature and applied strain rate, and homogeneous deformation normally occurs for $T_h > 0.65 \sim 0.70$ during quasi-static tensile or compressive tests. The T_h value of $La_{63.1}Al1_{5.2}(Cu,Ni)_{21.7}$ and $La_{64}Al_{14}$-$(Cu,Ni)_{22}$ BMG is 0.71 and 0.73, respectively. This means that the viscous flow may contribute to the plastic deformation at room temperature, which is proved by the appearance of creep during nanoindentation (Fig. 2). The time-dependent creep is suppressed during rapid loading and occurs mainly during the load-holding segment, whereas at low loading rates, creep occurs also during the loading process, which is proved by the lower average slope of the loading curves. The creep deformation is related to the localized viscous flow, and is thought to strongly affect of deformation behavior of the BMGs. The appearance of serrated flow is caused by the sudden release of elastic stress around the shear band due to the propagation of a single shear band. The viscous flow during nanoindentation in the BMGs with high T_h values will relax the elastic stress around the shear bands, and consequently produce a smoother P-h curve at low loading rates. In contrast, at high loading rates, the viscous flow is suppressed. Therefore the propagation of shear bands leads to a strong serration due to rapid release of elastic stress around the shear bands. As for the alloys with low T_h values, the contribution of viscous flow to the plastic deformation is limited. This is proved by the quite limited creep displacement during nanoindentation in these alloys (Fig. 2(a), 2(b)). Therefore, serrations with large size forms during nanoindentation because of the stress release around shear bands. At higher loading rates, the contribution of viscous flow is neglectable, and simultaneous operation of multiple shear bands leads to less prominent serrated flow during nanoindentation. Furthermore, the plastic deformation during indentation in the alloys with low T_h is only accommodated in the localized shear bands due to the lack of viscous flow, whereas in the alloys with high T_h, plastic deformation is partially accommodated by viscous flow. This may be the reason for the larger shear band number in low T_h alloys for the almost same overall plastic deformation during indentation as shown in Fig. 5.

4. Conclusions

Plastic deformation behavior of $La_{64}Al_{14}(Cu,Ni)_{22}$, $La_{63.1}$-$Al1_{5.2}(Cu,Ni)_{21.7}$, $La_{57.6}Al_{17.5}(Cu,Ni)_{24.9}$, and $La_{55}Al_{25}$-$Cu_{10}Ni_5Co_5$ BMGs with low glass transition temperatures is studied using nanoindentation. The four BMGs exhibit different rate dependency of serrated flow features. The BMGs with low homologous temperature (T_h) show prominent serrated flow at low loading rates and less pronounced serrated flow at high rates during nanoindentation, whereas the BMGs with high T_h exhibit a smooth loading curve at low rates and pronounced serrated flow at high rates. The changeover of the flow behavior occurs around $T_h = 0.69$. The different serrated flow feature in the two BMGs is ascribed to their difference in T_g, and consequently the contribution of viscous flow to the plastic deformation.

Acknowledgements

The authors acknowledge the support by the National Nature Science Foundation of China (Grant Nos. 50571109, 10572142 and 10432050) and the Knowledge Innovation Program of the Chinese Academy of Sciences.

REFERENCES

1) F. Spaepen: Acta Metall. **25** (1977) 407–415.
2) A. S. Argon: Acta Metall. **27** (1979) 47–58.
3) Y. Kawamura and A. Inoue: Appl. Phys. Lett. **77** (2000) 1114–1116.
4) H. S. Chen, H. Kato, A. Inoue, J. Saida and N. Nishiyama: Appl. Phys. Lett. **79** (2001) 60–62.
5) M. D. Demetriou and W. L. Johnson: J. Appl. Phys. **95** (2004) 2857–2865.
6) A. Reger-Leonhard, L. Q. Xing, M. Heilmaier, A. Gebert, J. Eckert and L. Schultz: Nanostructured Materials **10** (1998) 805–817.
7) Y. Kawamura, T. Shibata, A. Inoue and T. Masumoto: Acta Mater. **46** (1998) 253–263.
8) H. S. Chen: Script Metall. **7** (1973) 931–936.
9) W. J. Wright, R. Saha and W. D. Nix: Mater. Trans. **42** (2001) 642–649.
10) C. A. Schuh and T. G. Nieh: J. Mater. Res. **19** (2004) 46–57.
11) C. A. Schuh, A. C. Lund and T. G. Nieh: Acta Mater. **52** (2004) 5879–5891.
12) A. L. Greer, A. Castellero, S. V. Madge, I. T. Walker and J. R. Wilde: Mater. Sci. Engng. A **375–377** (2004) 1182–1185.
13) B. C. Wei, T. H. Zhang, W. H. Li, Y. F. Sun, Y. Yu and Y. R. Wang: Intermetallics **12** (2004) 1239–1243.
14) W. H. Li, T. H. Zhang, D. M. Xing, B. C. Wei, Y. R. Wang and Y. D. Dong: J. Mater. Res. **21** (2006) 75–81.
15) W. H. Jiang, F. E. Pinkerton and M. Atzmon: Acta Mater. **53** (2005) 3469–3477.
16) T. G. Nieh, C. A. Schuh, J. Wadsworth and Y. Li: Intermetallics **10** (2002) 1178–1182.
17) B. C. Wei, T. H. Zhang, L. C. Zhang, D. M. Xing, W. H. Li and Y. Liu: Mater. Sci. Eng. A **449–451** (2007) 962–965.
18) H. Tan, Y. Zhang, D. Ma, Y. P. Feng and Y. Li: Acta Mater. **51** (2003) 4551–4561.